Interannual Variations in Upper-Ocean Heat Content and Heat Transport Convergence in the Western North Atlantic

SHENFU DONG
Scripps Institution of Oceanography, University of California, San Diego, La Jolla, California

SUSAN L. HAUTALA
School of Oceanography, University of Washington, Seattle, Washington

KATHRYN A. KELLY
Applied Physics Laboratory, University of Washington, Seattle, Washington

(Manuscript received 20 June 2006, in final form 6 February 2007)

ABSTRACT

Subsurface temperature data in the western North Atlantic Ocean are analyzed to study the variations in the heat content above a fixed isotherm and contributions from surface heat fluxes and oceanic processes. The study region is chosen based on the data density; its northern boundary shifts with the Gulf Stream position and its southern boundary shifts to contain constant volume. The temperature profiles are objectively mapped to a uniform grid (0.5° latitude and longitude, 10 m in depth, and 3 months in time). The interannual variations in upper-ocean heat content show good agreement with the changes in the sea surface height from the Ocean Topography Experiment (TOPEX)/Poseidon altimeter; both indicate positive anomalies in 1994 and 1998–99 and negative anomalies in 1996–97. The interannual variations in surface heat fluxes cannot explain the changes in upper-ocean heat storage rate. On the contrary, a positive anomaly in heat released to the atmosphere corresponds to a positive upper-ocean heat content anomaly. The oceanic heat transport, mainly owing to the geostrophic advection, controls the interannual variations in heat storage rate, which suggests that geostrophic advection plays an important role in the air–sea heat exchange. The 18°C isotherm depth and layer thickness also show good correspondence to the upper-ocean heat content; a deep and thin 18°C layer corresponds to a positive heat content anomaly. The oceanic transport in each isotherm layer shows an annual cycle, converging heat in winter, and diverging in summer in a warm layer; it also shows interannual variations with the largest heat convergence occurring in even warmer layers during the period of large ocean-to-atmosphere flux.

1. Introduction

The large heat capacity of the ocean has prompted many questions regarding the heat exchange between the ocean and the atmosphere and the ocean's ability to store and transport heat. Upper-ocean heat content has been examined in a number of studies. However, many of those studies (e.g., Vonder Haar and Oort 1973; Ganachaud and Wunsch 2003) have focused on the seasonal cycle and the oceanic heat transport is estimated as a residual, owing in part to the lack of availability of subsurface temperature data and the data required to calculate the oceanic transport of heat, especially the geostrophic heat advection. Consequently, the study of the role of ocean circulation in climate change has been limited.

Sea surface temperature (SST) has been used widely to represent the ocean state in studies on air–sea interaction. Conclusions on the role of ocean and atmosphere in climate change are mostly from the relationship between SST and the atmospheric variables. Previous studies suggested that SST anomalies on interannual and shorter time scales are primarily generated by variations in the air–sea heat fluxes (Cayan 1992; Halliwell 1998; Delworth 1996; Seager et al. 2000; Alexander et al. 2000); however, on decadal and longer time scales, variations in SST are dominated by oceanic

Corresponding author address: Shenfu Dong, Scripps Institution of Oceanography, University of California, San Diego, 9500 Gilman Drive, Mail Code 0230, La Jolla, CA 92093-0230.
E-mail: shdong@ucsd.edu

DOI: 10.1175/2007JPO3645.1

processes (Grotzner et al. 1998; Halliwell 1998; Deser and Blackmon 1993; Kushnir 1994). There are two questions regarding these conclusions: 1) How well does the SST represent the upper-ocean climate state? And 2) because these studies were mostly carried out over the interior ocean where the ocean currents are weak, do these conclusions still hold for regions where the currents are strong?

Is SST a reasonable proxy for the upper-ocean state? While it is true that SST is a direct link between ocean and atmosphere, the interaction between the ocean and the atmosphere depends on the persistence of the SST anomaly. Subsurface temperature plays an important role in the "reemergence" of the SST anomaly from one winter to another through entrainment (Alexander and Deser 1995). A model study by Bhatt et al. (1998) suggested that the persistence of SST anomalies strongly depends on the subsurface temperature anomalies. The subsurface temperature better reflects how much heat is stored in the upper ocean. Deser et al. (2003) have suggested that the memory of the ocean is better reflected in the oceanic heat content than in the SST. The anomalous upper-ocean heat content indicates the total amount of heat that the ocean can release to the atmosphere. To understand the role of the ocean in climate change, it is necessary to understand what controls subsurface temperature, or even better, upper-ocean heat content, not just the SST.

The importance of the ocean in climate change depends not only on the amount of heat that the ocean can release to the atmosphere, but also on its heat transport. Heat carried by the ocean can be advected continually downstream or can be released to the atmosphere; it can also be stored in the ocean. There is a balance between the heat storage rate, the divergence of heat transport, and the surface fluxes. In most of the ocean, the surface fluxes play an important role in the variations in heat storage rate. However, the correlation between the surface fluxes and the heat storage rate is poor in the western subtropical gyre regions owing to the large heat transport by the western boundary currents. Recent studies using a simple three-dimensional thermodynamic model (Vivier et al. 2002; Dong and Kelly 2004) and in situ observations (Roemmich et al. 2005) have shown that oceanic heat transport is critical to the interannual variations in upper-ocean heat content in those regions. The oceanic heat transport includes two components: Ekman and geostrophic. Ekman transport has been considered to be the major contributor to ocean heat transport in many previous studies (Luksch 1996; Seager et al. 2000; Dong and Sutton 2001). On the other hand, geostrophic advection has received much less attention, because of either a lack of observations or the inaccuracy of ocean models. However, a three-dimensional thermodynamic model study (Dong and Kelly 2004) suggests that the largest variations in oceanic heat transport on interannual time scales are from changes in geostrophic heat transport. The observed variations in heat storage rate suggest that there may be a large volume divergence/convergence in different density layers, a hypothesis that we examine here. Because of a lack of salinity data, the density field is assumed to be well represented by the temperature field, an assumption that is reasonable for our study region in the upper subtropical gyre south of the Gulf Stream. The questions are: How does the subsurface thermal structure change corresponding to the changes in the upper-ocean heat content? In which isothermal layers does heat divergence/convergence occur?

The dominant feature of the upper-ocean thermal structure in the western North Atlantic Ocean is the Subtropical Mode Water (STMW), a vertically homogeneous water mass between the seasonal thermocline and the permanent thermocline. The STMW is formed by deep convection just south of the Gulf Stream (GS) during winter and contains the memory of its interaction with the atmosphere. After its formation, the STMW is advected by the GS and its recirculation gyre. The net heat loss to the atmosphere has been considered an important factor for forming and sustaining the STMW (Worthington 1959; Talley and Raymer 1982). However, previous studies (Warren 1972; Talley and Raymer 1982; Yasuda and Hanawa 1997) showed no direct correspondence between the net surface heat fluxes and the STMW properties, suggesting the importance of the ocean heat content in damping the effects of severe winters. Talley and Raymer (1982) found that the correlation between the heat fluxes and the STMW properties was opposite to what was expected: a smaller heat release to the atmosphere is associated with lower STMW temperature, higher density, and a large renewal rate. Yasuda and Hanawa (1997) found the same relationship between the surface heat flux and the North Pacific STMW properties: higher temperature is linked to the increased heat release from the ocean to the atmosphere. They attributed the large heat release to the increased warm water advection by the Kuroshio. Ocean advection plays an important role in the variations in upper-ocean heat content; does the ocean advection play a role in the volume changes of the mode water? And, what is the relationship between the STMW and the upper-ocean heat content?

To answer the above questions, we analyze the subsurface temperature data to evaluate the role of oceanic heat transport in variations in the upper-ocean heat

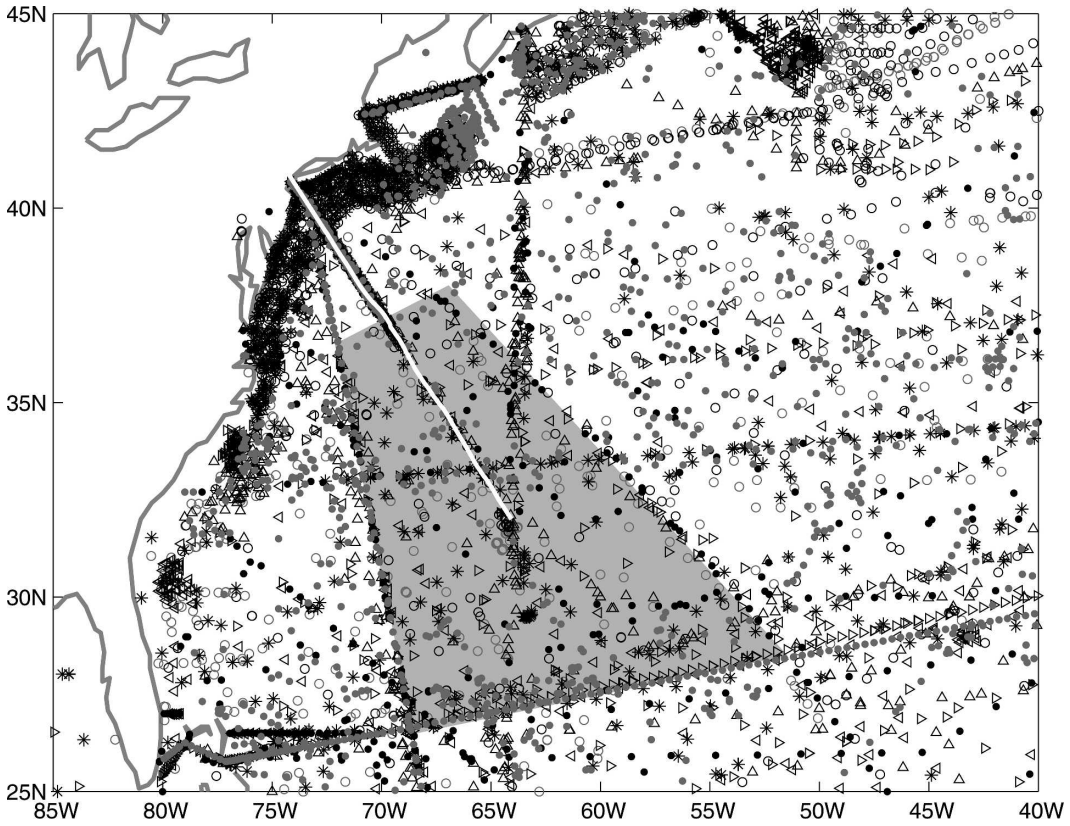

FIG. 1. Wintertime [January–March (JFM)] data distribution. The shaded area is our study region. The white line in the middle of our study region marks the *Oleander* section.

content and to examine variations in the subsurface thermal structure. The results are compared with that from the three-dimensional model of Dong and Kelly (2004). The data used in this study are described in the next section. In section 3, results from the subsurface data analysis are given. An inverse model is applied in section 4 to examine the convergence/divergence in isothermal layers. A discussion and conclusions are given in sections 5 and 6, respectively.

2. Data and processing

Three types of data are used in this analysis: subsurface temperature, sea surface height (SSH) measurements from the Ocean Topography Experiment (TOPEX)/Poseidon (T/P) altimeter, and daily and monthly National Centers for Environmental Prediction–National Center for Atmospheric Research (NCEP–NCAR) reanalysis products, which are described below.

a. Subsurface temperature

Temperature profiles from the Global Temperature-Salinity Profile Program (GTSPP) archive are analyzed to study heat content variations in the western North Atlantic from winter 1992 to 1999. Instruments used to collect the data include thermistor chains (on buoys), expendable bathythermographs (XBTs), digital bathythermographs (DBTs), bottle samplers, and conductivity–temperature–depth sensors (CTDs). Only data passing quality control are used. The major quality tests for the data include the following: 1) reasonableness of the position, the time, and the identification of a profile, 2) plausible values for the variables, 3) the consistency of the data with climatology, and 4) the internal consistency within the datasets. A detailed description of the GTSPP was available online (nodc.noaa.gov/GTSPP/index.html).

The geographical distribution of the temperature profiles (Fig. 1) in the western North Atlantic shows relatively heavy sampling along a few sections that are chosen as the boundaries of our study region. The temperature profiles are linearly interpolated in depth to every 10 m within the upper 800 m. Then, they are gridded into 0.5° latitude × 0.5° longitude × 1 month bins. Outliers (anomalies greater than two standard deviations in a bin) are eliminated. The number of the temperature profiles left is between 1000 and 2000 yr^{-1}

in our study region. The binned data are used to compute the spatial and temporal decorrelation scales. First, the monthly climatology from *World Ocean Atlas 2001* (*WOA01*; Conkright et al. 2002) is removed to calculate the temperature anomalies. This anomalous temperature is used to calculate the covariance for the maximum lags of 5° latitude, 10° longitude, 150 m in depth, and 12 months in time. A best fit for an exponential function, which decreases with increasing lag in each dimension, is derived from the covariance matrix, which gives *e*-folding scales of 1° latitude, 1.5° longitude, 150 m in depth, and 120 months in time. The temperature anomalies are then objectively mapped (Carter and Robinson 1987) onto a regular grid (0.5° latitude × 0.5° longitude × 10 m × 3 months) using the exponential covariance functions and a four-dimensional objective mapping procedure. Regions where there are no data available are excluded, which is less than 3% of our study region.

The decorrelation scales derived here are quite different from those derived by White (1995). The different scales can be attributed to regional differences and to the difference in data density. White (1995) used a relatively large grid size (2.5° latitude × 5° longitude × 3 months) for a global coverage. We focus on a small region with dense data, so we are able to use a small grid spacing.

b. Sea surface height

Changes in the SSH represent the variations in upper-ocean heat content if the contributions from barotropic changes, saline contraction, and deeper water steric response are relatively small. Previous studies (White and Tai 1995; Kelly et al. 1999) suggested that the variations in upper-ocean heat content from temperature profiles show good agreement with the changes in the T/P SSH. Thus, the SSH, as a proxy for upper-ocean heat content, is compared to the upper-ocean heat content derived from the objective maps to give an evaluation of the temperature field.

The T/P SSH maps are also used to calculate surface geostrophic velocity. The 10-day SSH map is an anomaly field, where the temporal mean sea level has been removed from the T/P measurements because of the unknown geoid. A mean SSH is needed to derive the mean geostrophic velocity. The mean SSH in the northwest Atlantic is reconstructed from the nearly 10-yr T/P altimeter along-track measurements based on the synthetic jet method (Kelly and Gille 1990; Qiu 1994) and combined with hydrographic data (Singh and Kelly 1997). The total SSH is obtained by adding this mean SSH to the SSH anomaly map. Details of the reconstruction procedure and the mean SSH were available online (kkelly.apl.washington.edu/projects/natl/). This synthetic jet method (Kelly and Gille 1990; Qiu 1994) also gives the GS position, which is used to determine the northern boundary of the study region to exclude the GS.

c. Atmospheric variables

The daily wind stress from the NCEP–NCAR reanalysis is used to compute Ekman transports across the boundaries. The Woods Hole Oceanographic Institution's objectively analyzed air–sea heat fluxes (OAFlux; Yu and Weller 2007) are used in the examination of the role of heat fluxes in determining the variations in upper-ocean heat content and in the inverse calculation to constrain the heat balance. Of the four components released in the OAFlux, the shortwave and longwave radiations are from the International Satellite Cloud Climatology Project (ISCCP; Zhang et al. 2004). Analysis using the latent and sensible heat fluxes computed from the Coupled Ocean–Atmosphere Response Experiment (COARE) algorithm (Fairall et al. 1996) and the longwave and shortwave radiations from the NCEP–NCAR reanalysis give the same results. The monthly wind speed, surface air temperature, and SST from the NCEP–NCAR reanalysis are used to examine their contributions to the changes in surface heat fluxes. All the data are averaged over 3-month periods to match the objective temperature maps.

3. Data analysis

The subsurface data analysis is carried out using the control volume shown in Fig. 1 (shaded region) bounded below by the 15.5°C isotherm, and on the east and west by lines of high data density. The 15.5°C isotherm is chosen as the bottom of the control volume owing to the relative stability of the thickness of the 16°C layer (bounded by 15.5° and 16.5°C isotherms) in time. The northern boundary is chosen to be 1.5° south of the GS center to eliminate direct GS influence. The southern boundary is shifted meridionally to maintain a fixed volume, which simplifies the interpretation of changes in heat content considerably. Comparison of results from a time-varying and a fixed boundary suggests that this choice has little impact on our conclusions.

In this section, we examine 1) interannual variations in the temperature distribution and comparisons with observed velocity and the SSH field; 2) interannual variations in the heat content and its relationship with

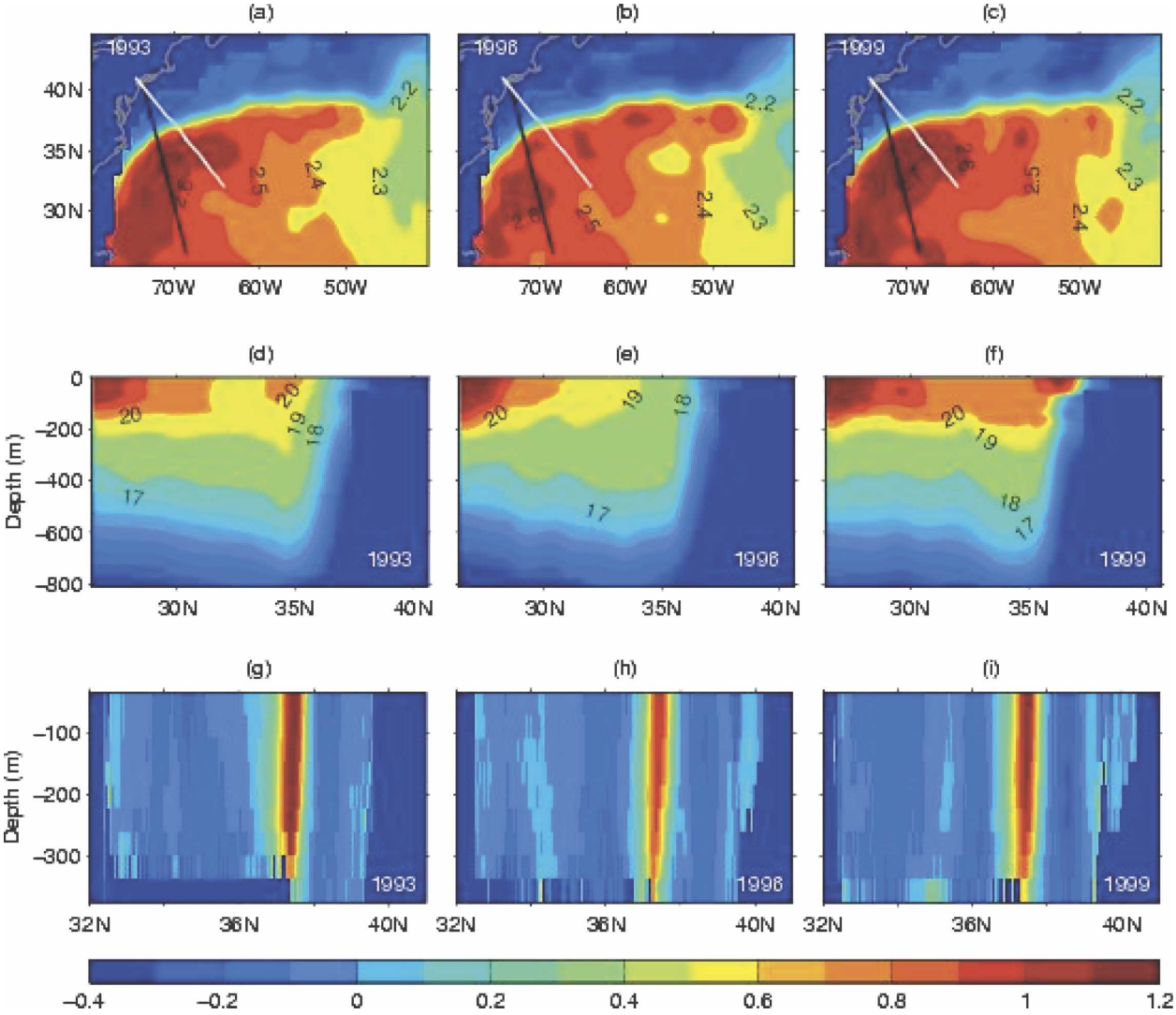

FIG. 2. JFM SSH (m) distribution for (a) 1993 ("elongated" GS), (b) 1996 ("contracted" GS), and (c) 1999 ("elongated" GS); (d)–(f) the corresponding temperature (°C) distributions along western section [black line in (a)] for the same three years in (a)–(c). (g)–(i) The zonal velocity (m s^{-1}) along the *Oleander* section [white line in (a)] for winter 1993, 1996, and 1999.

surface heat fluxes; 3) the relationship between subsurface thermal structure and upper-ocean heat content.

a. Comparison of subsurface and surface fields

We note that salinity also contributes to the SSH change (Sato et al. 2000). However, Sato et al. (2000) found that the saline corrections in the heat content estimation from SSH based on climatology give equivalent or worse results than not applying a correction. Since sufficient salinity measurements are not available, a salinity correction is not applied in this study.

Large-scale interannual variations in the SSH in the western subtropical gyre region have been observed in recent years. As described in Dong and Kelly (2004), the GS oscillates between two states: a stronger (weaker) GS is accompanied by an "elongated" ("contracted") region of high SSH, which is defined as an "elongated" ("contracted") GS state. For example, the GS is weak in 1996 with the high SSH confined to the west (Fig. 2b), whereas the eastward penetration of the high SSH in 1999 (Fig. 2c) corresponds to an "elongated" GS state. The temperature sections clearly show the corresponding interannual variations (Figs. 2d–f). The wintertime (January–March) temperature along the western section in 1999 (elongated state) is high compared to that in 1996 (contracted state). The warming in the GS elongated state is apparent from the 19°–20°C isotherm outcrops, which are shifted about 5° far-

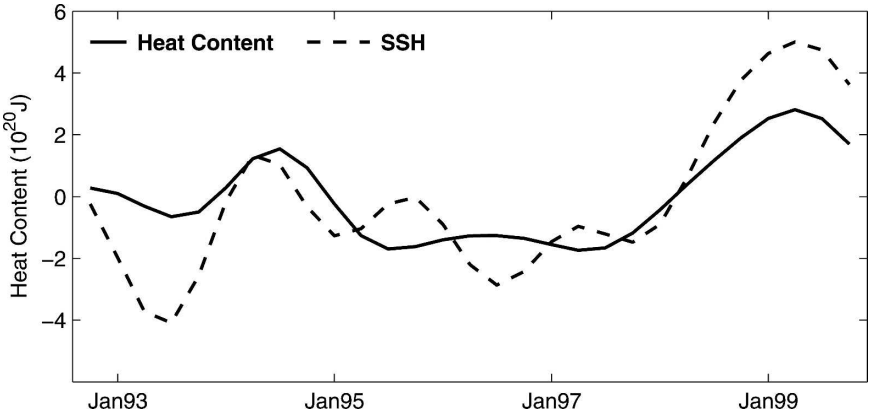

FIG. 3. Interannual variations in the domain-averaged upper-ocean heat content (solid) and that in the SSH (dashed), where the seasonal cycle is removed and a low-pass filter is applied to remove signals with periods of less than a year. SSH is converted to heat content unit (J) by multiplying by $\rho_0 c_p/\alpha$.

ther north in 1999 relative to that in 1996. The SSH map and temperature section in 1993 also indicate an elongated GS state, though both SSH and temperature are lower than those in 1999. This high–low–high variation from 1993 to 1999 indicates that the variations from 1996 to 1999 are not owing to a long-term trend. Similar variations are also seen along other sections (not shown).

In Fig. 2, we notice the deepening of the isotherms in a narrow region (34°–35°N) in 1999, which gives a strong thermal "wind" shear both north and south of this region with opposing signs. With the assumption that the reference velocity at a certain depth (deeper than 800 m) is unchanged, the stronger shear to the north in 1999 would give a large GS transport. The large opposing shear south of the GS (32°–34°N) suggests a stronger upper-ocean recirculation. These features are consistent with in situ ADCP observations (Figs. 2g–i) along the *Oleander* section (Rossby and Gottlieb 1998), which is located in the middle of our study region. The velocity distribution along the *Oleander* section indicates that the velocity of the GS is larger and that there is a stronger recirculation south of the GS (near 34°N) in 1993 and 1999, whereas in 1996 the GS is relatively weak.

The domain-averaged upper-ocean heat content from temperature maps shows good agreement with the SSH averaged over the same region on interannual time scales (Fig. 3), where the SSH has been converted to the same unit as heat content by multiplying by $\rho_0 c_p/\alpha$, where ρ_0 is the reference density of seawater, c_p is the specific heat of seawater at constant pressure, and α is the thermal expansion coefficient. A low-pass filter is applied to remove variations with periods less than a year. The interannual variations in SSH and in heat content are significantly correlated (0.8, 95% significant level is 0.6). Both the heat content and the SSH show positive anomalies in 1994, 1998, and 1999 and negative anomalies from 1995 to 1997. These variations are also consistent with the heat content derived from the thermodynamic model study (Dong and Kelly 2004).

These comparisons show that the SSH and subsurface temperature fields agree with one another very well, which suggests that surface observations from T/P primarily reflect variations in the upper-ocean temperature field.

b. *Interannual variations in the upper-ocean heat content and surface heat fluxes*

In the following analyses, we focus on interannual variations of domain-averaged properties (upper-ocean heat content, surface heat flux, and subsurface thermal structure). The seasonal cycle is removed and a low-pass filter is applied to remove signals with periods less than a year.

There are two major sources for heat content change: surface heating and ocean advection, as given by

$$\frac{\partial \mathrm{hc}}{\partial t} = \frac{Q_{\mathrm{net}}}{\rho_0 C_p} - \nabla \cdot (U_g T) - \nabla \cdot (U_e T) + \text{residual}, \quad (1)$$

where U_g and U_e are geostrophic transport and Ekman transport, respectively, hc is the heat content, Q_{net} is the net surface heat flux defined positive into the ocean, and T is temperature. The residual term includes processes other than surface heating and ocean advection (diapycnal mixing, diffusion). Previous studies (Vivier et al. 2002; Dong and Kelly 2004) have suggested that this residual term is small in the gyre regions, the heat content change being mainly controlled by surface heating and oceanic advection.

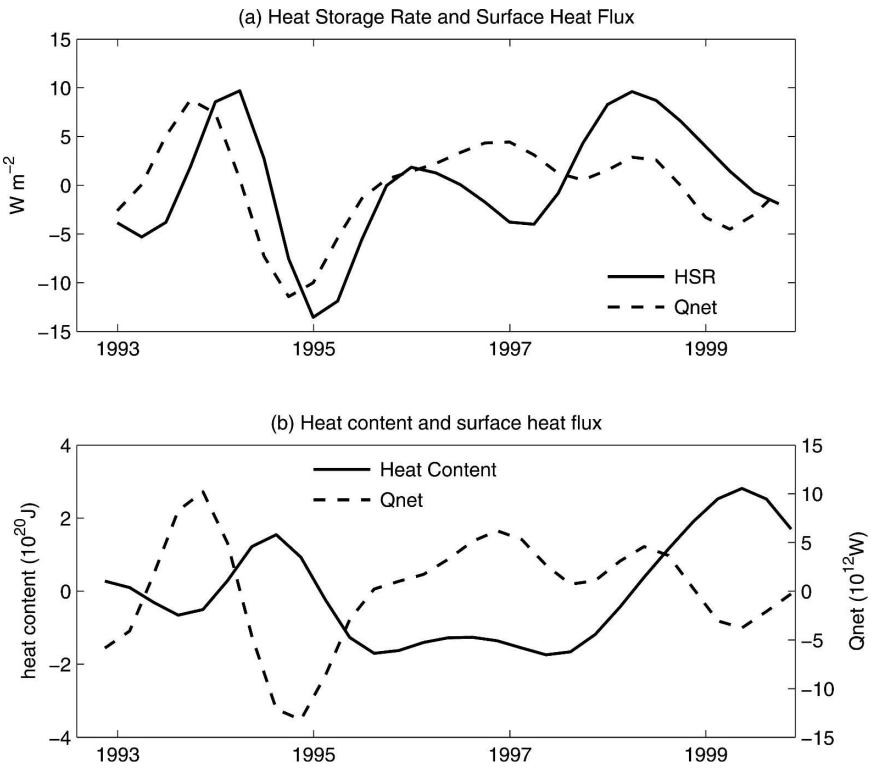

FIG. 4. Interannual variations in the domain-averaged (a) upper-ocean heat storage rate (solid) and surface heat fluxes (dashed) and (b) upper-ocean heat content (solid, left axis) and total sea surface heat fluxes in the study region (dashed, right axis). The seasonal cycle is removed and a low-pass filter is applied to remove signals with periods of less than a year.

The heat convergence terms [second and third terms on the right-hand side of (1)] include variations from isotherm motion owing to the convergence/divergence in each layer. So, changes in the upper-ocean heat content may be related to the movement of the thermocline, and hence the bottom boundary. However, comparison of the heat content above a fixed depth with that above the 15.5°C isotherm (not shown) indicates that the isotherm motion does not significantly influence the upper-ocean heat content.

Consistent with previous studies (Cayan 1992; Halliwell 1998; Seager et al. 2000), the seasonal cycle in heat content is controlled by the surface heating (not shown). However, changes in surface heat fluxes cannot explain the interannual variations in heat storage rate (Fig. 4a), consistent with results from the model studies (Vivier et al. 2002; Dong and Kelly 2004). The correlation between the heat storage rate and surface heat fluxes is nearly zero. Interestingly, the surface heat flux is negatively correlated ($\rho = -0.65$, above the 95% significance level of 0.59) with the upper-ocean heat content (Fig. 4b), so that high heat content corresponds to large heat losses from the ocean, suggesting that the ocean in our study region plays an active role in determining the interannual variations in air–sea heat flux. Of course, changes in the atmosphere (wind speed, surface air temperature) may also be responsible in part for the interannual variations in surface heat flux. To examine this relationship, we consider the sensible heat flux anomaly, which can be divided into two parts:

$$Q' \approx \beta(W\Delta T)' \approx \beta W'\overline{\Delta T} + \beta\overline{W}\Delta T',$$

where β is a constant, W is wind speed, and ΔT is the air–sea temperature difference ($\Delta T = T_{\text{air}} - T_{\text{ocean}}$). The overbar and prime denote the temporal mean and anomaly, respectively. A large heat release from the ocean to the atmosphere can come from a large wind speed or a large air–sea temperature difference. The anomalous surface fluxes owing to the wind speed changes ($\beta W'\overline{\Delta T}$) are small and are mostly in an opposite sense to that required to account for the variations in the surface heat flux (Fig. 5). The anomalous surface heat flux is highly correlated with ΔT (0.85; 95% significance level is 0.53), suggesting that the sensible heat flux changes are mostly owing to the air–sea temperature difference; T_{air} and T_{ocean} show similar interannual variations. However, T_{ocean} experiences rela-

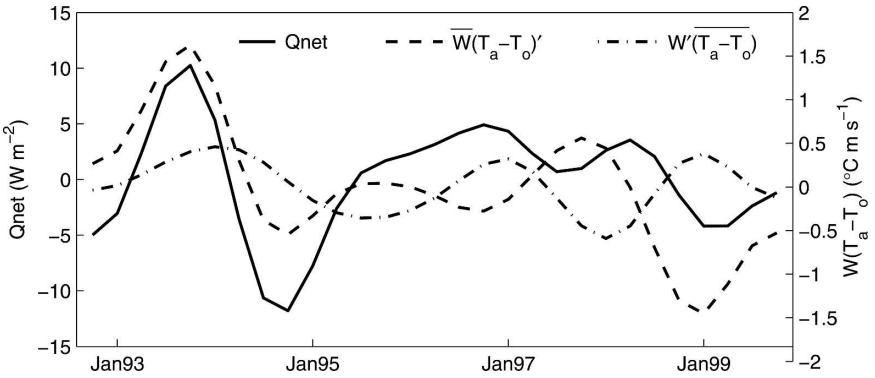

FIG. 5. Surface heat flux anomalies averaged in the study region (solid, left axis) and contributions from the air–sea temperature anomalies [$\overline{W}(T_a - T_o)'$, dashed, right axis] and from the wind speed anomalies [$W'(\overline{T_a - T_o})$, dash–dot, right axis].

tively large variability in comparison with T_{air}, which suggests that the ocean plays an important role in the surface heat fluxes on an interannual time scale. Similar examination of the latent heat flux anomaly shows that the specific humidity varies coherently with the latent heat flux except in 1993.

To summarize, the above analyses show that the changes in surface heat flux cannot explain the interannual variations in upper-ocean heat storage rate, which suggests that oceanic processes are important to variations in upper-ocean heat content. On the contrary, the upper-ocean heat content plays an important role in the surface heat flux through the air–sea temperature difference. Wind speed plays a small role in determining the surface heat flux anomalies in our study region.

c. Subsurface structure

One of our main objectives is to examine the relationship between the upper-ocean heat content and the subsurface thermal structure. A major feature of the western subtropical North Atlantic is the STMW, which is defined as the minimum stratification layer between the seasonal thermocline and the permanent thermocline. The mode water acts as a heat reservoir to damp the effects of extreme events (Warren 1972). Here we examine the relationship between the upper-ocean heat content and the STMW. Since only temperature is considered in this analysis, we cannot define the mode water from the minimum density stratification. Instead, we use a constant temperature layer to define mode water. Our temperature maps indicate that the 18°C layer (17.5°–18.5°C) is the thickest layer in our study region, therefore corresponding to the minimum stratification. Temperature profiles (Fig. 6) also indicated that the temperature of the thermostad is about 18°C. Thus, the thickness of the 18°C layer is used in this study as a proxy for the vertical extent of the STMW. An examination of the volume of each isotherm layer ($T_i \pm 0.5$°C) indicates that the largest variations are in the 19° and 18°C layers; these layer variations are negatively correlated. Defining water 18.5°C and below as the cold water layer, interannual variations in the 18°C layer explain 90% of the total variance of the cold water volume.

Interannual variations in the upper-ocean heat content and the thickness of the 18°C layer averaged in the

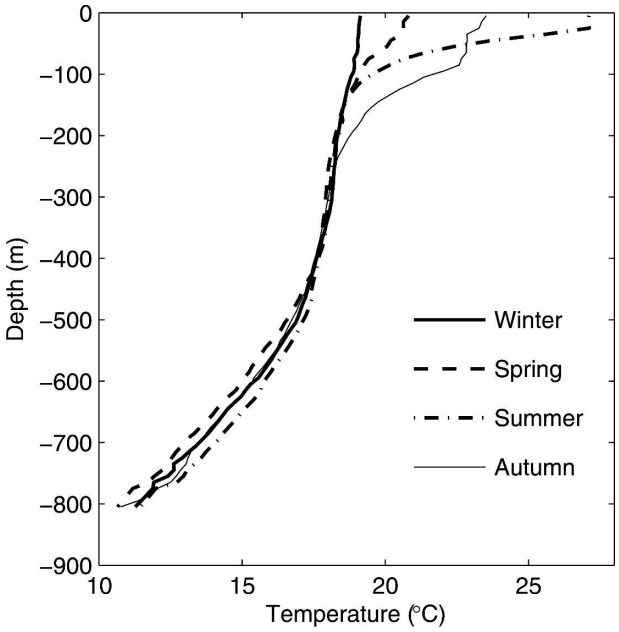

FIG. 6. Examples of temperature profiles at 36°N, 70°W in 1996 for winter (thick solid line), spring (dashed), summer (dash–dot), and autumn (thin solid).

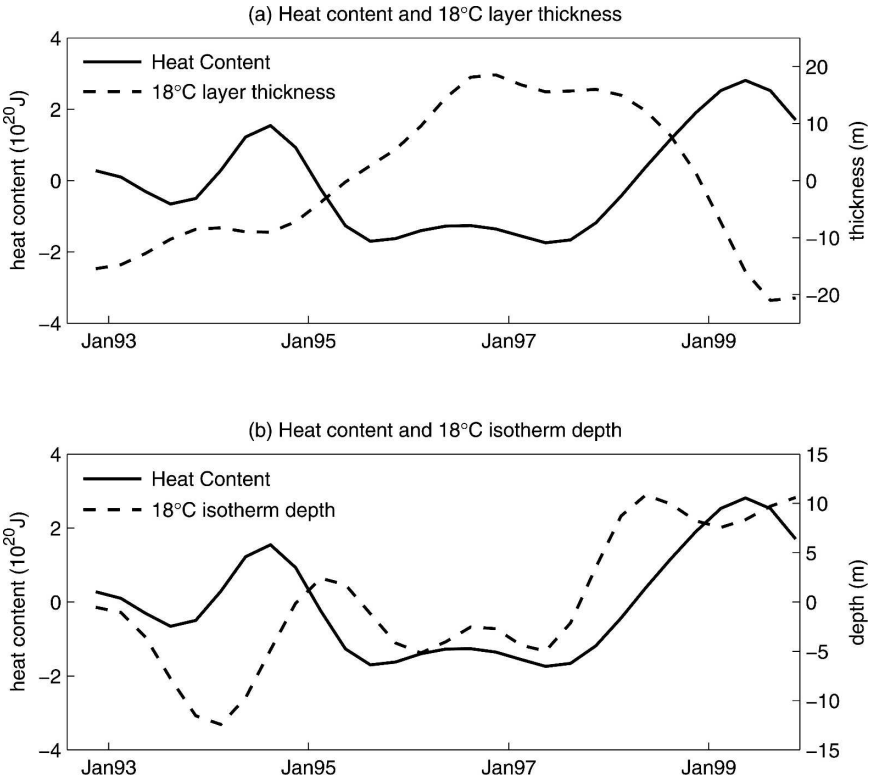

FIG. 7. Interannual variations in (a) upper-ocean heat content (solid, left axis) and 18°C layer thickness (dashed, right axis), and (b) upper-ocean heat content (solid, left axis) and 18°C isotherm depth (dashed, right axis). The seasonal cycle is removed and a low-pass filter is applied to remove signals with periods of less than a year.

box (Fig. 7a) show that a thick 18°C layer corresponds to a low heat content. The thickening from 1994 to 1997 and thinning afterward of the 18°C layer correspond well to the decreasing and increasing of the heat content, respectively, except in winter 1993/94 when the 18°C layer is thin and the heat content is low. In 1993/94 all isotherms are anomalously shallow corresponding to the cooling of the whole upper column, explaining the negative heat content anomalies. The interannual variations in the heat content and that in 18°C isotherm depth also show correspondence well (Fig. 7b): the 18°C isotherm deepens during a high heat content period. Overall, Fig. 7 suggests that a high heat content corresponds to a deep and thin 18°C layer, and vice versa. This relationship is different from Grey et al. (2000) who found that mode water is warm and has a large volume when the heat content is high. Kwon (2003) studied the North Atlantic STMW for a 40-yr period (1961–2000) with the traditional minimum potential vorticity (PV) definition and found that the volume of the mode water and the upper-ocean heat content are negatively correlated, consistent with our analysis. Our simple definition of the STMW and data limitation are unlikely to affect the conclusion about the relationship between the STMW and the heat content.

Next we examine the mechanisms for the variations in 18°C water (mode water). The formation of mode water has been considered a response to large air–sea heat fluxes and the resulting convection in the upper water column (Worthington 1959; McCartney 1982; Talley and Raymer 1982). An intuitive hypothesis is that a large heat loss to the atmosphere forms more mode water and decreases the upper-ocean heat content. Thus, more mode water is expected to be formed during a cold winter. However, we have shown in section 3b that a high heat content and thin 18°C layer (less mode water) correspond to a period of large heat release to the atmosphere, which is opposite to the above hypothesis. Thus, processes other than air–sea interaction must be more important in causing interannual variations in the volume of the 18°C water. Of the other processes, ocean advection is likely to be a major component. An alternative hypothesis is that a large advective convergence of cold water (<18.5°C) increases the volume of STMW and decreases the upper-

ocean heat content, which, in turn, causes less heat to be released to the overlying atmosphere. This hypothesis is examined in the next section using an inverse model.

4. Inverse method

To examine the role of lateral processes in the 18°C water variations, we examine the convergence/divergence of volume flux into isothermal layers. Oceanic advection includes two components: geostrophic and Ekman. Geostrophic transports in temperature layers can be computed by combining thermal "wind" shear with a reference surface geostrophic velocity derived from the altimetric SSH. The geostrophic velocity in an isothermal layer i is

$$u_{ig} = -\frac{g}{f}\frac{\partial \eta}{\partial y} + \sum_{j=1}^{i-1}\frac{g'}{f}\frac{\partial z_j}{\partial y}, \tag{2}$$

where η is the total sea surface height and z_i are the depths of a set of uniformly spaced (at interval $\Delta T = 1$°C) isotherms, g is gravitational acceleration, with reduced gravity $g' = \alpha \Delta T g$, α is the thermal expansion coefficient, and f is the Coriolis parameter. The isotherm depths are calculated from the objectively mapped temperature field. The second term on the right-hand-side is the accumulation of thermal "wind" shear above layer i. A detailed derivation of (2) is given in the appendix. The zonal geostrophic transport U_i through a meridional section in layer i is

$$U_{ig} = H_i \int_{y_s}^{y_0} u_{ig}\, dy = H_i\left(-\frac{g}{f}\Delta\eta + \sum_{j=1}^{i-1}\frac{g'}{f}\Delta z_j \right), \tag{3}$$

where H_i is the average thickness of layer i between y_s (the southern boundary) and y_0 (the outcrop of the corresponding isotherm or the northern boundary, whichever is smaller), and $\Delta\eta$ and Δz represent the difference of the SSH and that of the isotherm depth between y_s and y_0, respectively, with the convention that $z_j = 0$, and $\partial z_j/\partial y = 0$ north of an isotherm's outcrop. The transport across the southern boundary can be calculated the same way with respect to longitude.

As noted before, salinity is not considered in this study. Based on the *WOA01* monthly climatology (Conkright et al. 2002), the difference between the shear velocity with and without the salinity effect is small (less than 2 cm^{-1}), suggesting the salinity effect on the thermal "wind" shear is weak.

The Ekman transport U_e is determined from the wind stress as

$$U_e = \frac{\tau}{\rho_0 f} \times \hat{\boldsymbol{\kappa}}, \tag{4}$$

where τ is wind stress, and $\hat{\boldsymbol{\kappa}}$ is vertical unit vector, defined positive upward. The SST is used to compute heat transport by the Ekman velocity.

Because the reference level for geostrophic velocity is set at the sea surface, the "level of no motion" problem does not come up explicitly in our calculation. However, it is implicitly included in the reconstructed mean SSH, which incorporates hydrographic data and, in turn, affects the geostrophic advection calculation. A reference depth of 3000 m is used to extract the surface dynamic height from the Lozier/Owens/Curry HydroBase dataset (Lozier et al. 1995). Thus, away from the GS, when the synthetic jet model (Kelly and Gille 1990) is inadequate, the level of no motion is implicitly set at 3000-m depth. Although a direct estimate of ocean advection in each layer is possible with the available data, the error in the "level of no motion," together with the errors in the SSH and isotherm depths and with other processes ignored in (1), creates an imbalance between the heat storage rate, the surface heat fluxes, and the oceanic heat divergence. To estimate the contributions of ocean advection in the isothermal layers consistent with errors in the observations and to balance the heat budget, an inverse method is used to adjust velocity estimates in each layer.

a. Inverse formulation

The inverse calculation is carried out for each 3-month period to derive the correction to the velocity in each layer, which changes with time. The total geostrophic transport U_i in each isothermal layer is represented as a sum of that derived from (3) and a correction U_{ic} ($U_i = U_{ig} + U_{ic}$). Volume balance, heat balance, and constraints on the magnitude of the solution are combined to form a matrix inverse problem as follows:

$$\sum \boldsymbol{\nabla} \cdot U_i + \boldsymbol{\nabla} \cdot U_e = 0, \tag{5}$$

$$\varepsilon_1\left[\sum \boldsymbol{\nabla} \cdot (U_i T_i) + \boldsymbol{\nabla} \cdot (U_e T_s) + \frac{Q_{\text{net}}}{\rho_0 C_p} = \frac{\partial \text{hc}}{\partial t} \right], \tag{6}$$

$$\varepsilon_2 U_{ic} = 0, \quad i = 1, 2, 3, \ldots, n, \tag{7}$$

where Σ_i is the sum for all layers above the 15.5°C isotherm, T_s is the SST and T_i is the temperature of layer i, and ε_1 and ε_2 are the weighting factors for the heat balance and zero correction constraints, respectively. The inverse matrix formed by (5)–(7) is overde-

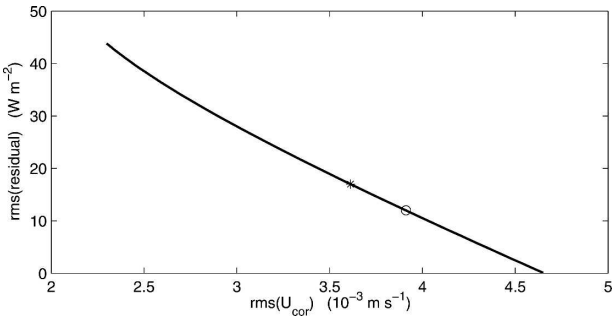

FIG. 8. Rms of the velocity corrections and the rms of the residual of the heat balance, which is assumed to be from errors in the surface heat fluxes. The star indicates the total rms of the residual in heat balance, and the circle corresponds to the rms of the ocean advection and surface heat flux residuals.

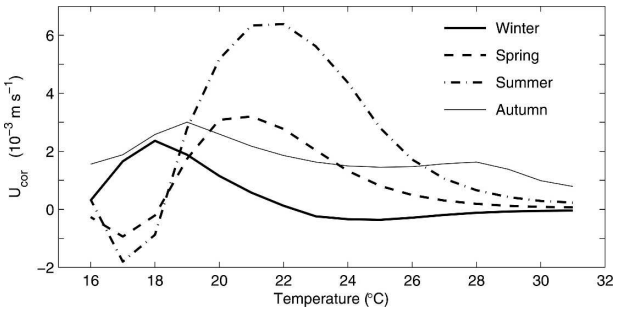

FIG. 9. Averages (10^{-3} m s^{-1}) of the velocity corrections at each temperature layer for winter (thick solid), spring (dashed), summer (dash–dot), and autumn (thin solid) for the western section.

termined for the corrections to horizontal velocity in each layer.

b. Velocity correction

The above inverse problem is solved for different constraints on the heat balance, that is, varying ε_1, which controls the size of the residual in (1) (imbalance in the heat balance). Here ε_2 is set to be the same order as the coefficient determined from (5), so that (5) and (7) have equal weight in the inverse problem. Figure 8 shows the root-mean-square (rms) of the residual in heat balance versus the rms of the velocity corrections. The residual decreases with increasing weight on the constraint ε_1. To estimate the residual, we compute the rms difference between the SSH (as a proxy for the observed heat content) and the heat content derived from the three-dimensional model study (Dong and Kelly 2004). The total rms difference is 17 W m^{-2}. Assuming that the ocean advection and the surface heat fluxes equally contribute to the residual, the rms error of each term is 12 W m^{-2}.

The corresponding corrections for the velocity are small (Fig. 8), less than 0.01 m s^{-1}, corresponding approximately to a 0.01-m SSH change in 1° latitude. The change of the correction with depth (or temperature) has a consistent structure for most years during the same season over our study period, but varies between seasons. Figure 9 shows the correction averaged for each season for the western section as an example; corrections for the eastern and southern sections are similar. The largest correction during winter is in the 18°C isotherm layers. The corrections in the warmer layers gradually increase from winter to summer. Relatively large corrections are seen in the 20°–24°C during summer. A positive correction corresponds to a convergence of water in the control volume.

c. Heat balance and volume convergence in isothermal layers

The upper-ocean heat balance (Fig. 10) can be calculated with the results of the inverse method. The surface heat fluxes in Fig. 10 are the sum of the surface heat fluxes from the OAFlux and the correction from the inverse method. The heat storage rate is closely related to lateral flux except during 1993–94, suggesting that the changes in upper-ocean heat storage rate are mostly from oceanic heat convergence. The Ekman heat transport across each boundary is negligible compared to the geostrophic heat transport. Although the Ekman and geostrophic components of the heat convergence in our study region are on the same order, the Ekman component is relatively small and opposite to the geostrophic component. As a result, the total heat convergence is significantly correlated with the geostrophic heat convergence, but not correlated with the Ekman heat convergence. Figures 4b and 10 together suggest that storage of warm water from the oceanic processes (mainly oceanic advection) controls the heat released into the atmosphere.

Next, we examine the volume convergence/divergence in each isothermal layer using the corrected velocity field. The volume convergence (Fig. 11) from the inverse model shows that the largest variations are in 18° and 19°C layers, consistent with the results of section 3 that the subsurface thermal structure is dominated by variations in 18° and 19°C isothermal layers. Another dominant feature in Fig. 11 is that the convergence in 18° and 19°C layers are opposite to each other, which is consistent with the negative correlation between the thickness of the two layers (not shown).

The interannual variations in volume convergence are related to the upper-ocean heat content and the surface heat fluxes: convergence in the warm layer increases the heat content of the water column; at the

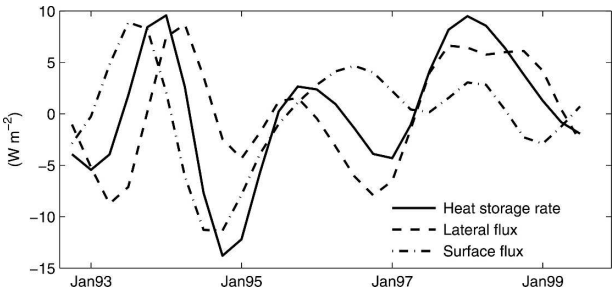

FIG. 10. Interannual variations in the upper-ocean heat storage rate (solid line) and contributions from the lateral flux (dashed) and sea surface flux (dash–dot). The seasonal cycle is removed and a low-pass filter is applied to remove signals with periods of less than a year.

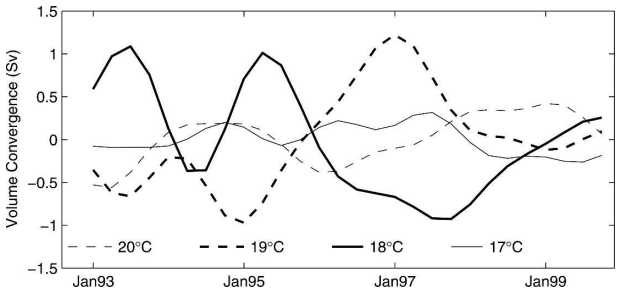

FIG. 11. Interannual variations [Sv (1 Sv $\equiv 10^6$ m^3 s^{-1})] in volume convergence in four isothermal layers: 20°C layer (thin dashed), 19°C layer (thick dashed), 18°C layer (thick solid), and 17°C layer (thin solid). The seasonal cycle is removed and a low-pass filter is applied to remove signals with periods of less than a year.

same time, heat is fluxed to the atmosphere, but not fast enough to keep the heat content steady. For example, the heat content has positive anomalies and the surface heat flux has negative anomalies (more heat loss to the atmosphere) in winter 1998 and 1999 (Fig. 4), and the heat convergence in the warmer layer is high, as shown for 20°C layer in Fig. 11. An increase in warm water volume means a decrease in cold water volume. There is more cold water moving out of the control volume during the period of positive heat content anomalies.

A detailed examination of the contribution of the ocean convergence to the volume changes in each isothermal layer is complicated owing to the errors. As a simplification, we divided the water column into warm (19°C and above) and cold (18°C and below) layers. Since the volume is conserved, the variations in the volume and ocean convergence in the warm layer mirror those in the cold layer exactly. Thus, only the variations in the cold layer are shown here (Fig. 12). It is clear that ocean advective convergence controls the interannual variations in the rate of change of the volume of this layer (Fig. 12), explaining 61% of the variance. There are large differences between the rate of change of volume and ocean convergence only in 1996 and 1999, which will be discussed in next section.

Of the other processes affecting volume change, conversion by surface heat fluxes is the major contributor. To examine the conversion between the warm and cold layers, we calculate the total surface heat fluxes in the outcrop region of the temperature that is most likely to be converted to cold water. The 3-month averaged temperature maps limit our analysis to autumn or winter. The water column during autumn is still highly stratified, and it is hard to determine the appropriate temperature outcrop region for mode water formation. So, we examine only the wintertime (January–March) temperature maps and suppose that there are two more months to cool the water column and form mode water. The water column is mixed down to about 200 m based on our wintertime maps. To cool a 200-m water column by 1°C in two months, the surface heat loss required from the ocean is about 160 W m^{-2}, which is reasonable based on the surface heat fluxes from the OAFlux. A 2°C temperature decrease would require 320 W m^{-2} heat release, which is too large. Thus, the 19°C outcrop area is used as the potential region to form mode water (18°C). Figure 13 shows that the variations in the difference between the rate of change of volume and the oceanic convergence (from Fig. 12) correspond reasonably well to the total surface heat flux anomalies over the 19°C outcrop region ($Q_t = \int Q_{\text{net}}\, dA$): more cold water (mode water) formation corresponds to a large total heat loss (negative values in Fig. 13).

5. Discussion

The large heat advection of the western boundary currents has been the subject of many studies recently (Yulaeva et al. 2001; Sutton and Mathieu 2002; Dawe and Thompson 2007) seeking a possible role for ocean advective heat convergence in midlatitude climate change. The inverse calculation here supports the conclusion from the thermodynamic model study of Dong and Kelly (2004): ocean advection dominates interannual variations in the heat storage rate. Thus, ocean advection plays an important role in the variations of the upper-ocean heat content. The data analysis suggests that the heat content anomaly from ocean advection determines the surface heat flux anomaly in the GS region. Yasuda and Hanawa (1997) found the same relationship between heat advection by the Kuroshio and surface heat fluxes. The question remains as to whether the air–sea heat exchange anomalies in the western gyre regions are large enough to change the atmo-

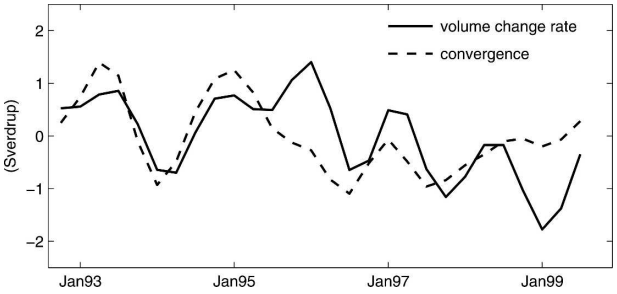

FIG. 12. The rate of change of the volume (solid line) and the convergence of ocean advection (dashed) for cold water layer (18°C and below).

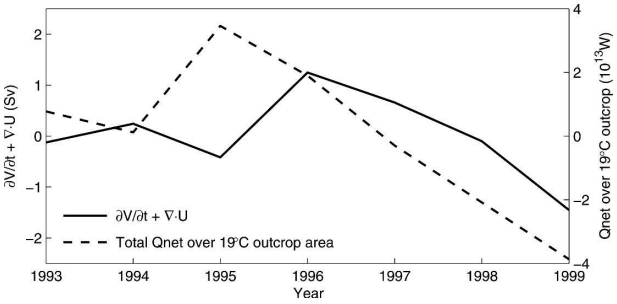

FIG. 13. JFM anomalies of the difference (solid, left axis) between the rate of change of volume of the cold water and the oceanic convergence (Sv), and the total surface heat flux (10^{13} W, dashed, right axis) over the 19°C outcrop area. The 19°C outcrop area is defined as the region bounded by 18.5° and 19.5°C isotherms.

spheric state and, if so, how does the atmosphere change with changes in the air–sea heat exchange? While answers to these questions are far from settled and are beyond the scope of the current study, Yulaeva et al. (2001) found that an idealized heat flux perturbation with maximum amplitude of 20 W m^{-2} over the Kuroshio Extension has a significant impact on the overlying atmosphere consistent with an important role for western boundary current heat advection in midlatitude climate variability.

Our analysis suggests that formation of 18°C water depends greatly on the surface temperature (preconditioning) in the formation region. During the years when the SST is too high, even with a large amount of heat released from the ocean to the atmosphere, the ocean still cannot be cooled enough to form 18°C water. Ladd and Thompson (2000, 2001) found that the initial stratification of the water column is very important in mode water formation. Although our study indicates that the ocean convergence usually controls changes of the volume of cold water, there are large differences between the rate of change of volume and ocean convergence in 1996 and 1999. Here we examine the average temperature for the upper 200-m water column along 35°N for fall 1995 and 1998, before the formation seasons of 1996 and 1999. The upper water column in fall 1998 is about 1°C warmer than that in fall 1995 (Fig. 14a). To lose this extra heat in 3 months, the ocean has to release >100 W m^{-2} ($\Delta Q = \rho c_p h \Delta T/\Delta t$) more heat in winter 1999 relative to winter 1996. Although the surface heat flux is about 50 W m^{-2} larger than in 1996, it is not large enough to remove all the extra heat. As a result, the temperature west of 50°W in winter 1999 (Fig. 14c) is still too warm to form 18°C water. However in 1996, even though the heat released from the ocean is small, the low upper-ocean temperature before winter allows more 18°C water formation. The temperature map along 35°N (Fig. 14b) clearly shows the outcrop of the 18°C water in our study region in 1996. In 1999, the outcrop of 18°C water shifts to the east of 50°W, which suggests that 18°C water might be formed farther to the east of our study region.

We showed in section 4 that the cold water conversion by surface heat fluxes corresponds well to the total surface heat flux over the 19°C outcrop region, Q_t. Interestingly, Q_t is controlled by the area of the outcrop region (Fig. 15), not by the mean magnitude of heat flux ($\overline{Q_{\text{net}}} = \int Q_{\text{net}}\, dA / \int dA$). The variations in $\overline{Q_{\text{net}}}$ are opposite to the anomalous Q_t, which again suggests the importance of preconditioning in forming mode water.

6. Summary

We present here an analysis of the interannual variations in the upper-ocean heat content in the western North Atlantic and its relation to the subsurface thermal structure from temperature profiles extracted from GTSPP. The objectively mapped temperature fields show good correspondence with satellite-observed SSH maps and in situ ADCP velocity observations.

Heat content shows positive anomalies in 1993–95, negative anomalies in 1996–97, and positive anomalies again during 1998–99. These interannual variations compare well with the T/P SSH and the upper 400-m heat content from a study using a thermodynamic model (Dong and Kelly 2004). The subsurface temperature distributions show interannual variations consistent with that observed in the SSH: the eastward extension of the high temperature in 1993 and 1999 corresponds to the "elongated" GS state (eastward extension of the high SSH). This indicates that the SSH reflects changes below the surface. Further analysis of the subsurface thermal structure indicates that the thickness and depth of the 18°C water (mode water) are well correlated with the upper-ocean heat content: the 18°C

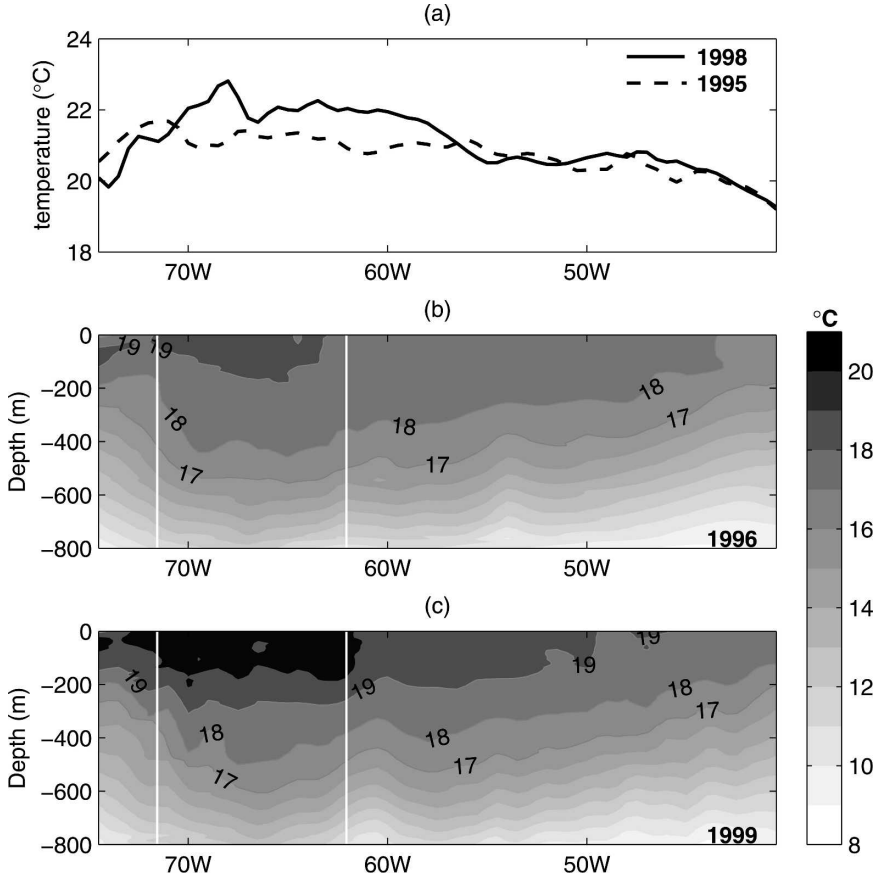

FIG. 14. (a) Temperature averaged for upper 200-m water column centered at 35°N (32.5°–37.5°N) for autumn 1995 (dashed) and 1998 (solid). JFM temperature distribution along 35°N for (b) 1996 and (c) 1999. White lines indicate the eastern and western boundaries of our study region.

layer is thin and deep during a high heat content period, and vice versa. One expects that changes in heat content and 18°C water volume are caused by surface heat fluxes: a large heat loss to the atmosphere would form more mode water and decrease heat content. However, our analysis shows a different scenario.

Changes in the surface heat flux cannot explain interannual variations in the heat storage rate in the GS region, a conclusion that is different from the interior ocean where ocean advection is small and surface heat flux plays a dominant role in changes in the upper-ocean heat storage rate. In the GS region, variations in the heat content and those in the surface heat fluxes are negatively correlated: a large heat loss from the ocean to the atmosphere corresponds to a high heat content. This negative correlation, together with the fact that the interannual variations in surface heat fluxes mostly come from the air–sea temperature difference, not from wind speed, suggests that the ocean's heat content controls heat release to the atmosphere.

The objectively mapped temperature is used to study the heat balance and interannual variations in the convergence/divergence of transport within isothermal layers in the region south of the GS. To accommodate several sources of error, we use an inverse method to

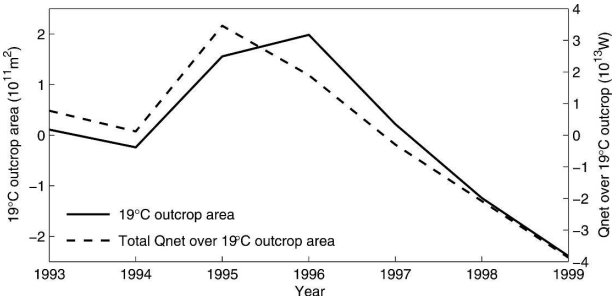

FIG. 15. JFM anomalies of the 19°C outcrop area (10^{11} m^2, solid, left axis) and the total surface heat fluxes in the 19°C outcrop region (10^{13} W, dashed, right axis). The 19°C outcrop area is defined as the region bounded by 18.5° and 19.5°C isotherms.

balance the heat and volume budgets. Analysis of the heat budget from the inverse model indicates that ocean advection dominates the interannual variations in upper-ocean heat storage rate, and hence, the heat content. Together with the negative correlation between heat content and surface heat fluxes, the dominance of ocean advection in the heat storage rate suggests that ocean advection in the GS region plays an important role in the air–sea interaction in the western subtropical gyre region.

An analysis by isothermal layers showed that variations in the volume of cold water (18°C and below, dominated by 18°C layer–mode water) are dominated by oceanic advective convergence, not by surface heat flux, suggesting that ocean advection plays an important role in the 18°C water volume changes. The difference between the volume change rate and ocean advective convergence (i.e., conversion) in the cold water is well correlated with the size of the 19°C outcrop area, which suggests the importance of preconditioning in mode water formation. The temperature distribution suggests that the 18°C water formation region shifts to the east during warm years and that no mode water is formed in our study region.

Acknowledgments. The authors thank Drs. LuAnne Thompson and Peter Rhines for their helpful comments. Special thanks are given also to the two anonymous reviewers for their helpful comments and suggestions. The ADCP data along *Oleander* section are provided by Dr. Tom Rossby. This study was supported by NSF through Grant OCE-0095688. KAK was supported by NASA Contract 1267196 with the University of Washington through Jet Propulsion Laboratory (Ocean Surface Topography Science Team).

APPENDIX

Divergence of Geostrophic Transport

The thermal–wind relationship between geostrophic velocity and temperature field often raises the question: How does the geostrophic current cause heat (or volume) divergence/convergence? Since the geostrophic velocity in isotherm layers (2) is not a standard expression, we show here how it is derived from the isotherm depths.

The pressure at any given depth, z, in layer i is given by

$$p(z) = p_0 + g\int_z^{\eta} \rho\, dz = p_0 + \rho_1 g\eta - \Delta\rho g(z_1 + z_2 + \ldots + z_{i-1}) - \rho_i g z, \quad \text{(A1)}$$

where p_0 is the surface pressure.

Thus, the geostrophic velocity in isotherm layer i is

$$u_{ig} = -\frac{1}{\rho_0 f}\frac{\partial p}{\partial y} = -\frac{g}{f}\frac{\partial \eta}{\partial y} + \sum_{j=1}^{i-1}\frac{g'}{f}\frac{\partial z_j}{\partial y}. \quad \text{(A2)}$$

The heat divergence/convergence in each isotherm layer is actually the volume divergence/convergence times the corresponding temperature:

$$\nabla\cdot(U_iT_i) = T_i\nabla\cdot U_i = T_i\nabla\cdot(u_iH_i), \quad \text{(A3)}$$

where T_i is the ith layer temperature, U_i is the geostrophic transport of layer i, and H_i is the layer thickness.

Substituting the geostrophic velocity (A2) in layer i, the volume divergence is

$$\nabla\cdot(u_iH_i) = u_i\cdot\nabla H_i = \frac{g}{f}\mathbf{J}(\eta, H_i) + \sum_{j=1}^{i-1}\frac{g'}{f}\mathbf{J}(z_j, H_i), \quad \text{(A4)}$$

where η and z_i are the sea surface height and the isotherm depth, and $\mathbf{J}(a, b)$ is the Jacobean. The Jacobean is zero when the gradients of a and b are parallel. The divergence of the geostrophic current in each isothermal layer is owing to the changes of the layer thickness. The geostrophic current will cause divergence or convergence as long as the thickness of the layer is not constant and the gradients of the depths of the isotherms above this layer and that of the sea surface are not parallel to the gradients of the thickness of this layer.

The total volume divergence above layer n is

$$\sum_i^n \nabla\cdot(u_iH_i) = \frac{g}{f}\mathbf{J}(\eta, H_n) + \sum_j^{n-1}\frac{g'}{f}\mathbf{J}(z_j, z_n), \quad \text{(A5)}$$

where $H_i = z_i - z_{i-1}$.

Thus, the total volume divergence of the geostrophic current is owing to the horizontal turning of the isotherms relative to the deepest isotherm; in other words, there would be no divergence or convergence from the geostrophic current if the horizontal gradients of the isotherm depths are parallel to the deepest isotherm depth. Bryden (1976) derived a similar representation of horizontal advection of temperature as a function of the speed and turning about the vertical of the horizontal current and suggested that this representation gives a good estimate of the horizontal advection of temperature.

REFERENCES

Alexander, M. A., and C. Deser, 1995: A mechanism for the recurrence of wintertime midlatitude SST anomalies. *J. Phys. Oceanogr.,* **25,** 122–137.

——, J. D. Scott, and C. Deser, 2000: Processes that influence sea surface temperature and ocean mixed layer depth variability in a coupled model. *J. Geophys. Res.,* **105,** 16 823–16 842.

Bhatt, U. S., M. A. Alexander, D. S. Battisti, D. D. Houghton,

and L. M. Keller, 1998: Atmosphere–ocean interaction in the North Atlantic: Near-surface climate variability. *J. Climate,* **11,** 1615–1632.

Bryden, H. L., 1976: Horizontal advection of temperature for low-frequency motions. *Deep-Sea Res.,* **23,** 1165–1174.

Carter, E. F., and A. R. Robinson, 1987: Analysis models for the estimation of oceanic fields. *J. Atmos. Oceanic Technol.,* **4,** 49–74.

Cayan, D. R., 1992: Latent and sensible heat flux anomalies over the northern oceans: Driving the sea surface temperature. *J. Phys. Oceanogr.,* **22,** 859–881.

Conkright, M. E., and Coauthors, 2002: *Introduction*. Vol. 1, *World Ocean Atlas 2001,* S. Levitus, Ed., NOAA Atlas NESDIS 42, U.S. Government Printing Office, 159 pp.

Dawe, J. T., and L. Thompson, 2007: PDO-related heat and temperature budget changes in a model of the North Pacific. *J. Climate,* **20,** 2092–2108.

Delworth, T. L., 1996: North Atlantic interannual variability in a coupled ocean–atmosphere model. *J. Climate,* **9,** 2356–2375.

Deser, C., and M. L. Blackmon, 1993: Surface climate variations over the North Atlantic Ocean during winter: 1900–1989. *J. Climate,* **6,** 1743–1753.

——, M. A. Alexander, and M. S. Timlin, 2003: Understanding the persistence of sea surface temperature anomalies in midlatitudes. *J. Climate,* **16,** 57–72.

Dong, B.-W., and R. T. Sutton, 2001: The dominant mechanisms of variability in Atlantic ocean heat transport in a coupled ocean-atmosphere GCM. *Geophys. Res. Lett.,* **28,** 2445–2448.

Dong, S., and K. A. Kelly, 2004: Heat budget in the Gulf Stream region: The importance of heat storage and advection. *J. Phys. Oceanogr.,* **34,** 1214–1231.

Fairall, C. W., E. F. Bradley, D. P. Rogers, J. B. Edson, and G. S. Young, 1996: Bulk parameterization of air-sea fluxes for Tropical Ocean-Global Atmosphere Coupled-Ocean Atmosphere Response Experiment. *J. Geophys. Res.,* **101,** 3747–3764.

Ganachaud, A., and C. Wunsch, 2003: Large-scale ocean heat and freshwater transports during the World Ocean Circulation Experiment. *J. Climate,* **16,** 696–705.

Grey, S. M., K. Haines, and A. Troccoli, 2000: A study of temperature changes in the upper North Atlantic: 1950–94. *J. Climate,* **13,** 2697–2711.

Grotzner, A., M. Latif, and T. P. Barnett, 1998: A decadal climate cycle in the North Atlantic Ocean as simulated by the ECHO coupled GCM. *J. Climate,* **11,** 831–847.

Halliwell, G. R., Jr., 1998: Simulation of North Atlantic decadal/mutidecadal winter SST anomalies driven by basin-scale atmospheric circulation anomalies. *J. Phys. Oceanogr.,* **28,** 5–21.

Kelly, K. A., and S. T. Gille, 1990: Gulf Stream surface transport and statistics at 69°W from the Geosat altimeter. *J. Geophys. Res.,* **95,** 3149–3161.

——, L. Thompson, and F. Vivier, 1999: Heat content changes in the Pacific Ocean. *Science,* **284,** 1735.

Kushnir, Y., 1994: Interdecadal variations in North Atlantic sea surface temperature and associated atmospheric conditions. *J. Climate,* **7,** 141–157.

Kwon, Y. O., 2003: Observation of general circulation and water mass variability in the North Atlantic subtropical mode water region. Ph.D. thesis, University of Washington, 161 pp.

Ladd, C., and L. Thompson, 2000: Formation mechanisms for North Pacific central and eastern subtropical mode waters. *J. Phys. Oceanogr.,* **30,** 868–887.

——, and ——, 2001: Water mass formation in an isopycnal model of the North Pacific. *J. Phys. Oceanogr.,* **31,** 1517–1537.

Lozier, M. S., W. B. Owen, and R. G. Curry, 1995: The climatology of the North Atlantic. *Prog. Oceanogr.,* **36,** 1–44.

Luksch, U., 1996: Simulation of North Atlantic low-frequency SST variability. *J. Climate,* **9,** 2083–2092.

McCartney, M. S., 1982: The subtropical recirculation of mode waters. *J. Mar. Res.,* **40** (Suppl.), 427–464.

Qiu, B., 1994: Determining the mean Gulf Stream and its recirculations through combining hydrographic and altimetric data. *J. Geophys. Res.,* **99,** 951–962.

Roemmich, D., J. Gilson, J. Willis, P. Sutton, and K. Ridgway, 2005: Closing the time-varying mass and heat budgets for large ocean areas: The Tasman box. *J. Climate,* **18,** 2330–2343.

Rossby, T., and E. Gottlieb, 1998: The *Oleander* Project: Monitoring the variability of the Gulf Stream and adjacent waters between New Jersey and Bermuda. *Bull. Amer. Meteor. Soc.,* **79,** 5–18.

Sato, O. T., P. S. Polito, and W. T. Liu, 2000: Importance of salinity measurements in the heat storage estimation from TOPEX/POSEIDON. *Geophys. Res. Lett.,* **27,** 549–551.

Seager, R., Y. Kushnir, M. Visbeck, N. Naik, J. Miller, G. Krahmann, and H. Cullen, 2000: Causes of Atlantic Ocean climate variability between 1958 and 1998. *J. Climate,* **13,** 2845–2862.

Singh, S., and K. A. Kelly, 1997: Monthly maps of sea surface height in the North Atlantic and zonal indices for the Gulf Stream using TOPEX/Poseidon altimeter data. Woods Hole Oceanographic Institution Tech. Rep. WHOI-97-06, 48 pp.

Sutton, R., and P. P. Mathieu, 2002: Response of the atmosphere-ocean mixed-layer system to anomalous ocean heat-flux convergence. *Quart. J. Roy. Meteor. Soc.,* **128,** 1259–1275.

Talley, L. D., and M. E. Raymer, 1982: Eighteen degree water variability. *J. Mar. Res.,* **40,** 757–775.

Vivier, F., K. A. Kelly, and L. Thompson, 2002: Heat budget of the Kuroshio Extension region: 1993–99. *J. Phys. Oceanogr.,* **32,** 3436–3454.

Vonder Haar, T. H., and A. H. Oort, 1973: New estimate of annual poleward energy transport by Northern Hemisphere oceans. *J. Phys. Oceanogr.,* **3,** 169–172.

Warren, B. A., 1972: Insensitivity of subtropical mode water characteristics to meteorological fluctuations. *Deep-Sea Res.,* **19,** 1–19.

White, W. B., 1995: Design of a global observing system for gyre-scale upper ocean temperature variability. *Prog. Oceanogr.,* **36,** 169–217.

——, and C.-K. Tai, 1995: Inferring interannual changes in global upper ocean heat storage from TOPEX altimetry. *J. Geophys. Res.,* **100,** 24 934–24 954.

Worthington, L. V., 1959: The 18°C water in the Sargasso Sea. *Deep-Sea Res.,* **5,** 297–305.

Yasuda, T., and K. Hanawa, 1997: Decadal changes in the mode waters in the midlatitude North Pacific. *J. Phys. Oceanogr.,* **27,** 858–870.

Yu, L., and R. A. Weller, 2007: Objectively analyzed air–sea heat fluxes for the global ice-free oceans (1981–2005). *Bull. Amer. Meteor. Soc.,* **88,** 527–539.

Yulaeva, E., N. Schneider, D. W. Pierce, and T. P. Barnett, 2001: Modeling of North Pacific climate variability forced by oceanic heat flux anomalies. *J. Climate,* **14,** 4027–4046.

Zhang, Y., W. B. Rossow, A. A. Lacis, V. Oinas, and M. I. Mishchenko, 2004: Calculation of radiative fluxes from the surface to top of atmosphere based on ISCCP and other global data sets: Refinements of the radiative transfer model and the input data. *J. Geophys. Res.,* **109,** D19105, doi:10.1029/2003JD004457.